

Technology Center (<http://sequence-www.stanford.edu/group/candida/index.html>). There are single homologues for each gene (the gene sequences for *C. albicans* *ICL1* and *MLS1* are deposited in GenBank under accession numbers AF222905 and AF222907, respectively). For northern analysis, macrophage interactions were performed as described above using  $10^6$  J774A cells in 5 ml media with  $2 \times 10^7$  *S. cerevisiae* (EM93) or *C. albicans* (SC5314) cells. Control populations were grown for 3 h in rich media (YPD), or in tissue culture media without (RPMI) or with (serum) 10% fetal bovine serum. Species-specific probes were amplified by PCR and labelled with a random primer.

**Mutant construction and analysis**

*Saccharomyces cerevisiae*  $\Delta icl1$  mutants were constructed in the EM93 background using a PCR-mediated protocol with a G418-resistance cassette<sup>13</sup>. Mutants were constructed in both mating types and mated to produce a homozygous  $\Delta icl1/\Delta icl1$  knockout strain (MLY283a/ $\alpha$ ). For *C. albicans*, an  $\Delta icl1$  disruption construct was created by inserting a *hisG-URA3-hisG* cassette<sup>14</sup> at a *Bgl*II site in the *ICL1* open reading frame. This construct was linearized, transformed into CA14 (a *Ura*<sup>-</sup> derivative of strain SC5314; refs 14, 15), and selected by uracil prototrophy. Accurate integrants were identified by PCR and passaged on 5-FOA medium. A second round of transformation was used to generate two independent homozygous  $\Delta icl1/\Delta icl1$  strains (MLC7 and MLC8; MLC7 was used for most of the experiments reported here). The wild-type *ICL1* gene was re-introduced on linearized plasmid pRC2312 (ref. 16) by transformation to produce a complemented strain (MLC10). *Candida albicans* transformations were done as described<sup>17</sup>. Standard media was used<sup>18</sup> and strains were grown at 37 °C unless otherwise indicated.

**Murine virulence assay**

Overnight cultures of *C. albicans* strains were diluted into fresh YPD and grown for 3–4 h at 37 °C. Cultures were collected by centrifugation and washed with PBS. Cells ( $6 \times 10^5$ ) were injected into the tail vein of 18–20-week-old female BALB/c mice. We used ten mice per strain. Mice were monitored for three weeks after injection and moribund animals were killed. We cared for animals according to NIH guidelines.

Received 9 February; accepted 8 May 2001.

1. Ashman, R. B. & Papadimitriou, J. M. Production and function of cytokines in natural and acquired immunity to *Candida albicans* infection. *Microbiol. Rev.* **59**, 646–672 (1995).
2. Lo, H. J. et al. Nonfilamentous *C. albicans* mutants are avirulent. *Cell* **90**, 939–949 (1997).
3. Wright, W. L. & Wenzel, R. P. Nosocomial *Candida*. Epidemiology, transmission, and prevention. *Infect. Dis. Clin. North. Am.* **11**, 411–425 (1997).
4. Bodey, G. et al. Fungal infections in cancer patients: an international autopsy survey. *Eur. J. Clin. Microbiol. Infect. Dis.* **11**, 99–109 (1992).
5. McKinney, J. D. et al. Persistence of *Mycobacterium tuberculosis* in macrophages and mice requires the glyoxylate shunt enzyme isocitrate lyase. *Nature* **406**, 735–738 (2000).
6. Honer Zu Bentrup, K., Miczak, A., Swenson, D. L. & Russell, D. G. Characterization of activity and expression of isocitrate lyase in *Mycobacterium avium* and *Mycobacterium tuberculosis*. *J. Bacteriol.* **181**, 7161–7167 (1999).
7. Kujaw, M., Weber, H. & Barth, G. Characterization of mutants of the yeast *Yarrowia lipolytica* defective in acetyl-coenzyme A synthetase. *Yeast* **8**, 193–203 (1992).
8. Tzschoppe, K., Augstein, A., Bauer, R., Kohlwein, S. D. & Barth, G. trans-dominant mutations in the *GPR1* gene cause high sensitivity to acetic acid and ethanol in the yeast *Yarrowia lipolytica*. *Yeast* **15**, 1645–1656 (1999).
9. Sedivy, J. M. & Fraenkel, D. G. Fructose biphosphatase of *Saccharomyces cerevisiae*. Cloning, disruption and regulation of the *FBP1* structural gene. *J. Mol. Biol.* **186**, 307–319 (1985).
10. Minard, K. I. & McAlister-Henn, L. Isolation, nucleotide sequence analysis, and disruption of the *MDH2* gene from *Saccharomyces cerevisiae*: evidence for three isozymes of yeast malate dehydrogenase. *Mol. Cell. Biol.* **11**, 370–380 (1991).
11. Mortimer, R. K. & Johnston, J. R. Genealogy of principal strains of the yeast genetic stock center. *Genetics* **113**, 35–43 (1986).
12. Wodicka, L., Dong, H., Mittmann, M., Ho, M. H. & Lockhart, D. J. Genome-wide expression monitoring in *Saccharomyces cerevisiae*. *Nature Biotechnol.* **15**, 1359–1367 (1997).
13. Wach, A., Brachat, A., Pohlmann, R. & Philippsen, P. New heterologous modules for classical or PCR-based gene disruptions in *Saccharomyces cerevisiae*. *Yeast* **10**, 1793–1808 (1994).
14. Fonzi, W. A. & Irwin, M. Y. Isogenic strain construction and gene mapping in *Candida albicans*. *Genetics* **134**, 717–728 (1993).
15. Gillum, A. M., Tsay, E. Y. & Kirsch, D. R. Isolation of the *Candida albicans* gene for orotidine-5'-phosphate decarboxylase by complementation of *S. cerevisiae* *ura3* and *E. coli* *pyrF* mutations. *Mol. Gen. Genet.* **198**, 179–182 (1984).
16. Cannon, R. D., Jenkinson, H. F. & Shepherd, M. G. Cloning and expression of *Candida albicans* *ADE2* and proteinase genes on a replicative plasmid in *C. albicans* and in *Saccharomyces cerevisiae*. *Mol. Gen. Genet.* **235**, 453–457 (1992).
17. Braun, B. R. & Johnson, A. D. Control of filament formation in *Candida albicans* by the transcriptional repressor TUP1. *Science* **277**, 105–109 (1997).
18. Sherman, F. Getting started with yeast. *Methods Enzymol.* **194**, 3–21 (1991).

**Acknowledgements**

We are grateful to G. Acton and E. Lander for access to microarray facilities; T. Galitski, A. Saldhana, C. Huff and F. Lewitter for help with informatics resources; and members of the Fink laboratory for useful discussions. This work was supported by NIH grants. G.R.F. is an American Cancer Society Professor of Genetics. M.C.L. is a post-doctoral fellow of the Irvington Institute for Immunological Research.

Correspondence and requests for materials should be addressed to G.R.F. (e-mail: fink@wi.mit.edu).

**Insights into Wnt binding and signalling from the structures of two Frizzled cysteine-rich domains**

Charles E. Dann\*, Jen-Chih Hsieh†‡, Amir Rattner†‡, Divya Sharma\*, Jeremy Nathans†‡§ & Daniel J. Leahy\*‡

\* Department of Biophysics and Biophysical Chemistry, † Department of Molecular Biology and Genetics, ‡ Howard Hughes Medical Institute, § Departments of Neuroscience and Ophthalmology, Johns Hopkins University School of Medicine, Baltimore, Maryland 21205, USA

Members of the Frizzled family of seven-pass transmembrane proteins serve as receptors for Wnt signalling proteins<sup>1</sup>. Wnt proteins have important roles in the differentiation and patterning of diverse tissues during animal development<sup>2,3</sup>, and inappropriate activation of Wnt signalling pathways is a key feature of many cancers<sup>4</sup>. An extracellular cysteine-rich domain (CRD) at the amino terminus of Frizzled proteins binds Wnt proteins<sup>1</sup>, as do homologous domains in soluble proteins—termed secreted Frizzled-related proteins<sup>5</sup>—that function as antagonists of Wnt signalling<sup>6–8</sup>. Recently, an LDL-receptor-related protein has been shown to function as a co-receptor for Wnt proteins and to bind to a Frizzled CRD in a Wnt-dependent manner<sup>9–11</sup>. To investigate the molecular nature of the Wnt signalling complex, we determined the crystal structures of the CRDs from mouse Frizzled 8 and secreted Frizzled-related protein 3. Here we show a previously unknown protein fold, and the design and interpretation of CRD mutations that identify a Wnt-binding site. CRDs exhibit a conserved dimer interface that may be a feature of Wnt signalling. This work provides a framework for studies of homologous CRDs in proteins including muscle-specific kinase and Smoothed, a component of the Hedgehog signalling pathway<sup>12,13</sup>.

The CRDs of secreted Frizzled-related protein 3 (sFRP-3) and mouse Frizzled 8 (mFz8), which possess 10 conserved cysteines within a domain of 120–125 amino acids, were expressed in Chinese hamster ovary (CHO) cells as a fusion with human growth hormone<sup>14</sup>. Putative N-linked glycosylation sites were eliminated by mutation, a step that proved essential to obtain diffraction-quality crystals. After cleavage of the fusion protein, mutant CRDs (CRDM) exhibited the same affinity for *Xenopus* Wnt-8 (XWnt8) as native CRDs and produced crystals that diffracted beyond 2.0 Å Bragg spacings. The structure of sFRP-3 CRDM was solved by multi-wavelength anomalous diffraction<sup>15</sup> using the anomalous signal from bound solvent bromide ions<sup>16</sup>. Nine bromide ions provided sufficient phasing for structure determination without non-crystallographic symmetry averaging despite the presence of six molecules (relative molecular mass 84,000 (*M<sub>r</sub>* 84K)) in the asymmetric unit. The structure of mFz8 CRDM was determined by molecular replacement using a truncated sFRP-3 CRDM as a search model.

The CRDM structures (Fig. 1a, b) are predominantly  $\alpha$ -helical with all cysteines forming disulphide bonds (Cys3–Cys64, Cys11–Cys57, Cys48–Cys87, Cys76–Cys115, Cys80–Cys104 in sFRP-3). The program DALI<sup>17</sup> and inspection of SCOP<sup>18</sup> and CATH<sup>19</sup> failed to identify a clear structural homologue, although visual inspection hints at a distant relationship to four-helix bundles. In addition to helical regions, two short  $\beta$ -strands at the N terminus form a minimal  $\beta$ -sheet with  $\beta 2$  passing through a knot created by disulphide bonds. The sFRP-3 and mFz8 CRDs are arranged as homologous dimers within the crystallographic asymmetric units with  $\sim 1,500 \text{ \AA}^2$  and  $\sim 900 \text{ \AA}^2$  buried, respectively, at a highly complementary dimer interface (Fig. 1c, d). Shape complementarity analysis of sFRP-3 and mFz8 dimers with the program SC showed values (0.71 and 0.64, respectively) consistent with known

protein–protein interfaces<sup>20</sup>. Both purified CRDs are, however, monomeric in solution at 100  $\mu$ M as judged by gel filtration chromatography, indicating a dissociation constant for the dimers between this value and 50 mM, the concentration of the CRDs in the crystals.

Several studies indicate a direct interaction between Wnt proteins and Frizzled or sFRP CRDs<sup>1,5,7,21</sup>. To identify regions of the CRD important for Wnt binding, we used a binding assay<sup>21</sup> *in vitro* and three mutagenesis strategies: tripeptide insertion, alanine scanning and homologue scanning<sup>22</sup>. In the binding experiments, the CRD was displayed on the surface of transiently transfected cells by a Myc-tagged glycosylphosphatidylinositol (GPI) anchor; and the cell-surface binding of a soluble *Xenopus* Wnt8–alkaline phosphatase fusion protein (XWnt8–AP) measured histochemically (Fig. 2). All of the mutants studied localized efficiently to the plasma membrane, as determined by immunostaining of living cells with anti-Myc antibody and release of the CRD–Myc fusion protein from the surface of living cells with phosphoinositide-phospholipase C. CRDs of *Drosophila* Frizzled 2 (DFz2) and mFz8 were used in these experiments because they exhibit a high affinity for XWnt8.

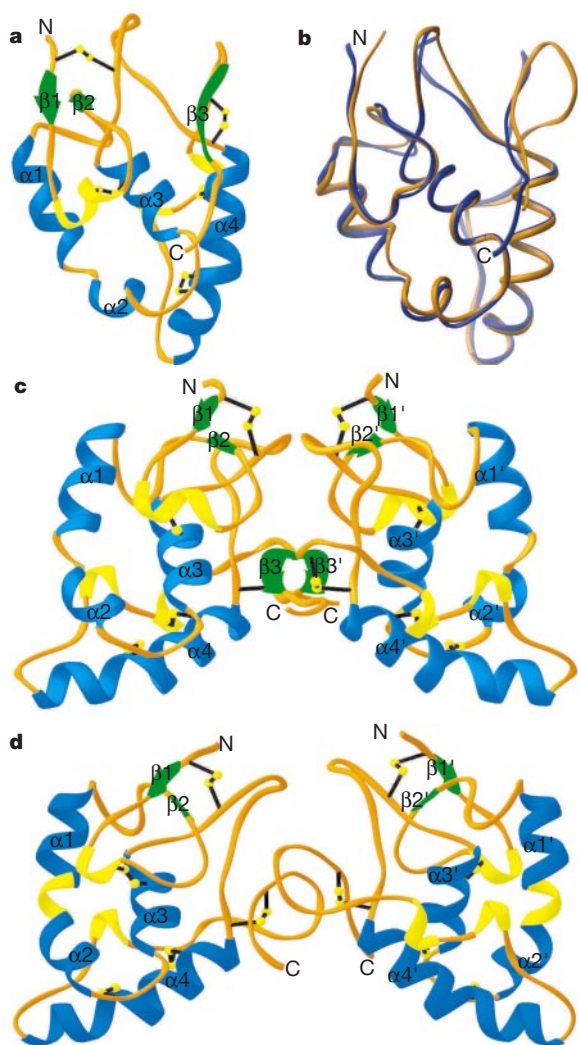


**Figure 1** Crystal structure of the sFRP-3 and mFz8 CRDs. **a**, Ribbon diagram of the sFRP-3 CRD with elements of secondary structure numbered in order of appearance in the primary structure. **b**, Superposition of sFRP-3 CRD (blue) and mFz8 CRD (brown). **c**, Dimer of the sFRP-3 CRD observed in the crystal. **d**, Dimer of the mFz8 CRD observed in the crystal. **a**, **c**, **d**,  $\alpha$ -helices, blue;  $3_{10}$ -helices, yellow;  $\beta$ -strands, green; coil, gold. Disulphide bonds are shown as ball-and-stick models in yellow and black. Images were generated by RIBBONS<sup>28</sup>.

Given their homologous structure and function, we presume that all Frizzled CRDs will bind Wnt proteins in a conserved fashion.

In earlier efforts to analyse Wnt–CRD binding, a series of 23 tripeptide insertions were constructed in the DFz2 CRD<sup>21</sup>. Guided by the sFRP-3 crystal structure, 11 additional tripeptide insertions were constructed in the DFz2 CRD to complete coverage of the CRD surface. The insertion sites for the entire set of 34 mutants and a summary of their effects on Wnt binding are shown in Fig. 3. The 16 insertion mutants that retain XWnt8–AP binding most likely reside in regions that do not make direct Wnt–CRD contacts (Fig. 3, green arrowheads; Fig. 4a, green areas). In general, members of this class of insertions were located within surface loops. Interpretation of the 18 insertion mutants that disrupt binding (Fig. 3, red arrowheads) is less clear. Whereas some insertions may directly block binding, many reside in regions of secondary structure and could affect binding indirectly through more global effects.

As a second approach to define the regions of the CRD that are involved in Wnt binding, we identified discrete surfaces on the CRD structure, and solvent-exposed residues constituting these surfaces in the mFz8 CRD were mutated *en bloc* to alanine. The sites of 15 different sets of alanine scanning mutations and their effects on XWnt8–AP binding are indicated in Fig. 3, and their positions on the CRD surface are shown in Fig. 4b. Most alanine scanning mutants had no effect on XWnt8–AP binding (green underlined symbols in Fig. 3), two blocks of mutations eliminated XWnt8–AP binding (red boxed symbols in Fig. 3), and three blocks greatly reduced binding (orange boxed symbols in Fig. 3).

The third method for identifying regions of the mFz8 CRD involved in Wnt binding exploited the inability of mouse Frizzled 6 (mFz6) or the isolated mFz6 CRD to bind XWnt8–AP<sup>21</sup>. Eight clusters of residues from the mFz6 CRD that occupy surface positions of the CRD and differ substantially in sequence from the corresponding regions of mFz8 were substituted for the homologous residues in mFz8, and the resulting mFz8/mFz6 chimaeras were assayed for XWnt8–AP binding (Figs 3 and 4c). Two substitutions resulted in a loss of XWnt8 binding, and these occurred within regions identified by the alanine scanning mutations as important for XWnt8–AP binding. One mFz8/mFz6 substitution in the region of the  $\alpha$ 4 helix that had no effect on binding largely overlapped an alanine scanning mutation with reduced binding.

The three mutagenesis strategies produced maps of the CRD surface regions involved in Wnt binding that are in good agreement

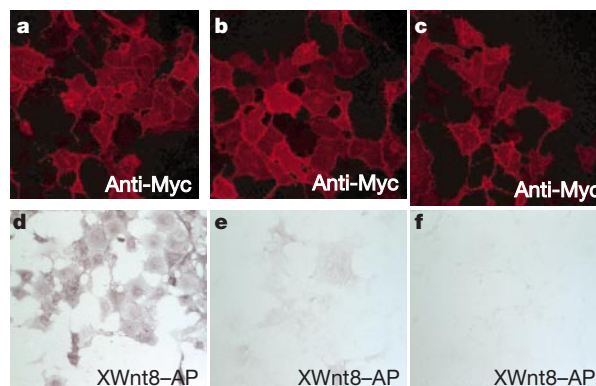


**Figure 2** Binding of XWnt8–AP to mFz8 CRD–Myc–GPI displayed on the surface of transfected COS cells. COS cells were transiently transfected with an alanine scanning mutant encompassing either mFz8 residues 114–118, which bound XWnt8–AP (**a**, **d**), mFz8 residues 17–25, which showed reduced XWnt8–AP binding (**b**, **e**), or mFz8 residues 17–23, which did not bind XWnt8–AP (**c**, **f**). **a–c**, Immunostaining of cell-surface mFz8 CRD–Myc–GPI in living (that is, nonpermeabilized) cells with anti-Myc monoclonal antibody followed by Texas red-conjugated secondary antibody. Confocal image at 2  $\mu$ m thickness. **d–f**, XWnt8–AP binding as seen with alkaline phosphatase histochemistry.

and that strongly implicate a single region of the CRD surface, comprising three segments of the primary sequence, as important for Wnt binding (Fig. 4). The simplest interpretation of these experiments is that this surface is the site of direct contact between Wnt and CRD molecules. The implicated region of the CRD surface (950 Å<sup>2</sup>) could reasonably contact a single Wnt molecule (*M<sub>r</sub>* ~45K). As a portion of the surface important for Wnt binding overlaps with the interface of the CRD dimer observed in the crystal, an alternative mechanism is suggested in which a subset of mutations may interfere with Wnt binding by hindering CRD dimerization.

Although no current evidence implicates dimerization of Wnt or

Frizzled proteins, the presence of the same dimer interface in the crystals of both sFRP-3 and mFz8 CRDs suggests that CRD dimerization may be of biological significance. Specifically, weak dimerization affinities of isolated CRDs may reflect dimerization induced by ligands and/or co-receptors as a feature of the signalling mechanism. As one test of this possibility, a solid-phase assay was developed that measures the XWnt8-dependent association of two differentially tagged mFz8 CRDs. In this assay, incubation with XWnt8-containing conditioned medium led to a >90-fold increase

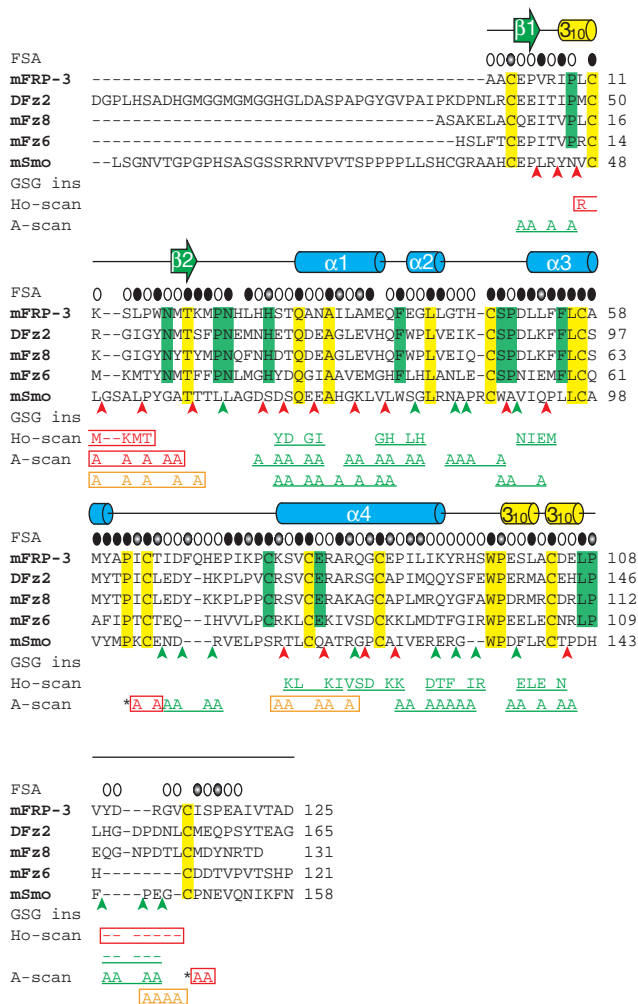


**Figure 3** Structure-based alignment of CRD sequences indicating sites altered by mutagenesis. Residues conserved in the Frizzled and Smoothened families (yellow) or only in the Frizzled family (green) are indicated. Fractional solvent accessibility (FSA) is indicated above each residue for which sFRP-3 and mFz8 have similar accessibility: filled ovals for buried residues (<10% exposed); partially filled ovals for moderately exposed residues (10–40% exposed); open ovals for exposed residues (>40% exposed). GSG ins, sites of Gly-Ser-Gly tripeptide insertions (DFz2 CRD): red arrowheads, insertion sites that eliminate XWnt8–AP binding; green arrowheads, sites that do not affect XWnt8–AP binding. Ho-scan, sites of homologue scanning mutagenesis (mFz6 CRD into mFz8 CRD); A-scan, alanine scanning mutagenesis (mFz8 CRD): residues mutated *en bloc* are indicated by an underline or a box; mutations that do not affect (green), that diminish (orange) or that abolish (red) XWnt8–AP binding are indicated. mSmo, mouse Smoothened. Asterisk, two blocks adjacent in the tertiary structure and therefore constructed together as a single alanine mutation set. Sequences of the mature proteins were deduced from known signal-peptide cleavage sites and sites predicted by the program SignalP<sup>29</sup>.

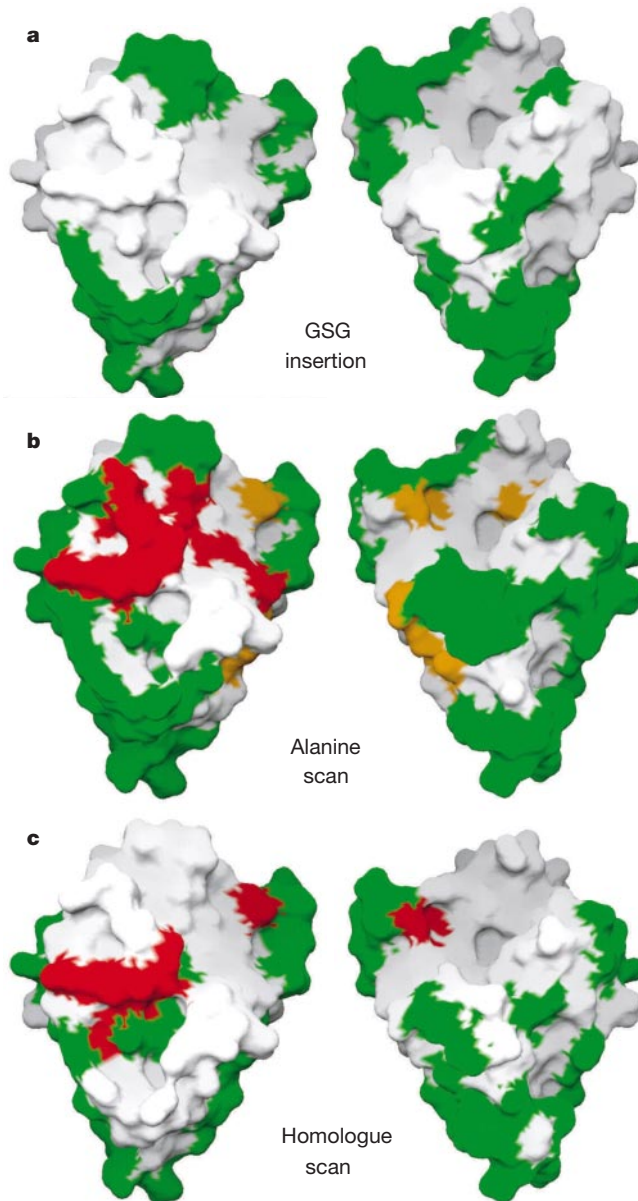


**Figure 4** Surfaces involved in Wnt–CRD interactions modelled on the mFz8 CRD structure. Mutations that do not affect binding (green), that produce weak binding (orange) and that disrupt binding (red) are indicated. The orientation of the CRD surface on the left is identical to the ribbon diagrams in Fig. 1b; the orientation on the right is rotated 180° about a vertical axis. **a**, Locations of the 16 Gly-Ser-Gly (GSG) insertions in the DFz2 CRD that did not affect binding to XWnt8–AP (green indicates the two amino acids that flank the point of insertion). **b**, Alanine scanning mutations in the mFz8 CRD. Alanine substitution of residues 117 and 118 (green) in the mFz8 CRD permitted binding when associated with two alanine substitutions upstream of this location, but not when associated with two alanine substitutions downstream. **c**, Homologue scanning mutations for mFz6/mFz8 CRD. Deletion of residues 114–120 in the mFz8 CRD eliminates binding, but deletion of residues 114–118 (green) does not. Images were generated by GRASP<sup>30</sup>.

in association of the tagged CRDs compared with control conditioned medium. The interpretation of this observation is uncertain, however, because the stoichiometry and composition of the CRD–Wnt complex formed in the assay is unknown. The majority of the XWnt8 present in conditioned medium is found in a large complex ( $M_r > 600K$ ) as judged by gel filtration. Although these results are consistent with the possibility that Wnt-induced multimerization of Frizzled receptors is involved in Wnt signalling, a definitive test of this hypothesis must await the development of biochemically defined preparations of Wnt proteins.

The crystal structures of the CRDs reported here are the first for any member of this large class of homologous domains found in many important signalling molecules<sup>12,13</sup> and appear to define a new protein fold. We used these structures to identify a surface on the CRD that is important for Wnt binding and we observed a dimer of both sFRP-3 and mFz8 CRDs that may be relevant to the mechanism of Wnt binding and signalling. These structures will allow a molecular understanding of Wnt–CRD specificity as more information concerning biological Wnt–CRD pairings becomes available, and will provide a framework for models of Wnt–CRD signal transduction. Finally, as the conserved cysteines permit accurate alignment of highly divergent CRD sequences (Fig. 3), the CRD structures provide a reliable model for studies of distantly related CRDs, such those found in muscle-specific kinase and Smoothed<sup>12,13</sup>, the functional roles of which are not known. □

## Methods

### Protein expression, purification and crystallization

Full-length complementary DNA from mouse sFRP-3 was subcloned into the pCIS vector and transfected into CHO cells using Lipofectin (Qiagen), and sFRP-3 protein was purified from conditioned serum-free medium (Ex-Cell 301, JRH Biosciences) by Mono-S cation exchange and heparin affinity chromatography (Pharmacia). Treatment of sFRP-3 with subtilisin results in a stable fragment that no longer binds heparin. N-terminal sequencing and mass spectrometry revealed this fragment to be the CRD. Full-length sFRP-3 did not crystallize, but the sFRP-3 CRD crystallized following enzymatic deglycosylation. The diffraction limit of these crystals depended on the level of deglycosylation but never extended beyond 7 Å. Asn 17 of sFRP-3 CRD (residues 1–125) was therefore mutated to Glu to eliminate the single N-linked glycosylation site; this mutant (sFRP-3 CRDM) was expressed in Chinese hamster ovary cells as a fusion protein with human growth hormone, an octahistidine tag, and a cleavage site for tobacco etch virus (TEV) protease<sup>14</sup>. This fusion protein was produced at 2.1 mg l<sup>-1</sup> and was initially purified by batch Ni-NTA immobilized metal affinity chromatography (Qiagen). The fusion protein was then cleaved by TEV protease, which leaves an additional Gly-Ser at the N terminus of the sFRP-3 CRDM. sFRP-3 CRDM was purified by gel filtration and ReSource Q anion exchange chromatography (Pharmacia) before concentration to 15 mg ml<sup>-1</sup> in deionized H<sub>2</sub>O for crystallization trials. mFz8 CRDM protein was expressed and purified in the same manner as sFRP-3 CRDM with the mutations N22E and N125E at putative glycosylation sites. All crystals were grown by vapour diffusion from hanging drops. For sFRP-3 CRDM, equal amounts of protein and a solution of 0.1 M HEPES and 12% PEG 3350 at pH 6.6 were mixed, suspended over this PEG solution, and equilibrated at 20 °C. sFRP-3 CRDM crystallized in space group P2<sub>1</sub> with cell dimensions  $a = 96.05 \text{ \AA}$ ,  $b = 46.79 \text{ \AA}$ ,  $c = 83.31 \text{ \AA}$  and  $\beta = 90.8^\circ$ . mFz8 CRDM crystals were grown using 0.1 M HEPES and 1.9 M (NH<sub>4</sub>)<sub>2</sub>SO<sub>4</sub> at pH 7.3 as mother liquor. mFz8 CRDM crystallized in space group P2 with cell dimensions  $a = 55.69 \text{ \AA}$ ,  $b = 36.37 \text{ \AA}$ ,  $c = 57.94 \text{ \AA}$  and  $\beta = 98.82^\circ$ .

### Structure determination

All data were collected at beamline X4A of the National Synchrotron Light Source at Brookhaven National Laboratory. To introduce bromide ions for phasing<sup>16</sup>, sFRP-3 CRDM crystals were first transferred stepwise to buffer containing 0.1 M HEPES and 33% PEG 3350 at pH 6.6 and then transferred to the same buffer containing 0.5 M NaBr for 40 s before flash freezing in a nitrogen stream at 100 K. mFz8 CRDM crystals were flash frozen in a nitrogen stream after transfer to mineral oil. Diffraction data from crystals were collected at 100 K and processed with the program HKL<sup>23</sup>. Nine solvent bromides were located and used for sFRP-3 CRDM phase determination with the program SOLVE<sup>24</sup>. Phases were improved by solvent flattening and phase extension with the program DM<sup>25</sup>. The program O was used for model building<sup>26</sup>, and refinement was performed with the CNS package and maximum likelihood targets<sup>27</sup>. Non-crystallographic symmetry restraints were used during early stages of the sFRP-3 CRDM refinement but relaxed when differences between molecules in the asymmetric unit became apparent. All refinements were carried out on data collected from a native crystal. Excluding the carboxy-terminal 5 residues, which extended away from the CRD and adopted multiple conformations, the six independent sFRP-3 CRD structures were essentially identical. The maximal pairwise root-mean-square deviation (RMSD) of alpha carbon distances between the six molecules in the asymmetric unit was 0.53 Å. The sFRP-3 CRDM with the lowest average B-factor and an ordered C terminus was chosen for display. mFz8 CRDM was solved by molecular

replacement using a sFRP-3 CRDM model in which all non-identical surface residues were truncated to alanine and the two structurally distinct loops removed. Of 122 alpha carbons of the mFz8 and sFRP-3 CRDs, 101 superimposed with a RMSD of 0.97 Å (Fig. 1b). Refinement and model building of mFz8 CRDM were carried out in the same manner as for the sFRP-3 CRDM without non-crystallographic symmetry restraints. The crystallographic  $R_{\text{work}}/R_{\text{free}}$  are 22.0/25.7 (30–1.9 Å) and 22.5/24.7 (30–1.35 Å), and the RMSD for bonds/angles are 0.0087 Å/1.48° and 0.0048 Å/1.29° for sFRP-3 and mFz8, respectively. Additional data collection and refinement statistics are available in the Supplementary Information.

### Binding of XWnt8–AP to DFz2 and mFz8 CRD mutants

DFz2 CRD residues 1–248 and mFz8 CRD residues 1–146 were transiently expressed in COS cells as an N-terminal fusion to a Myc epitope tag and a GPI anchor. Tripeptide insertions (DFz2 CRD), alanine and homologue scanning mutants (mFz8 CRD) were expressed, and binding assays performed as described<sup>1</sup>. Briefly, CRD-transfected COS cells were incubated with conditioned medium containing XWnt8–AP, washed, fixed and stained with alkaline phosphatase substrates. Binding quality was assigned visually relative to native CRD binding to XWnt8–AP. Normal binding was equivalent to native, weak binding was any level less than native, and non-binding was undetectable activity of alkaline phosphatase.

### Solid-phase assay of mFz8 CRD dimers

Plates with 96 wells (Corning) were coated with anti-hGH monoclonal antibody (ATCC) at 1 µg ml<sup>-1</sup> and blocked with 1% dialysed calf serum. Plates were then washed with PBS and 0.1% Tween-20 at pH 7.4 (PBS-T), and 3 µg of purified hGH-mFz8 CRD fusion protein was added. After incubation at 37 °C for 1 h, plates were washed with PBS-T, and 100 µl of either XWnt8–Myc or control S2 cell conditioned medium was added. After 15 min, 100 µl conditioned medium containing mFz8 CRD–AP expressed in transfected 293 cells was added, and the plates incubated for 45 min at 37 °C. Plates were then washed eight times with PBS-T, and the presence of mFz8 CRD–AP was detected using Blue Phos (Kirkegaard and Perry Laboratories).

Received 30 March; accepted 4 May 2001.

- Bhanot, P. *et al.* A new member of the frizzled family from *Drosophila* functions as a Wingless receptor. *Nature* **382**, 225–230 (1996).
- Nusse, R. & Varmus, H. E. Wnt genes. *Cell* **69**, 1073–1087 (1992).
- Wodarz, A. & Nusse, R. Mechanisms of Wnt signalling in development. *Annu. Rev. Cell Dev. Biol.* **14**, 59–88 (1998).
- Sparks, A. B., Morin, P. J., Vogelstein, B. & Kinzler, K. W. Mutational analysis of the APC/beta-catenin/Tcf pathway in colorectal cancer. *Cancer Res.* **58**, 1130–1134 (1998).
- Rattner, A. *et al.* A family of secreted proteins contains homology to the cysteine-rich ligand-binding domain of frizzled receptors. *Proc. Natl Acad. Sci. USA* **94**, 2859–2863 (1997).
- Finch, P. W. *et al.* Purification and molecular cloning of a secreted, Frizzled-related antagonist of Wnt action. *Proc. Natl Acad. Sci. USA* **94**, 6770–6775 (1997).
- Leyns, L., Bouwmeester, T., Kim, S. H., Piccolo, S. & De Robertis, E. M. Frzb-1 is a secreted antagonist of Wnt signalling expressed in the Spemann organizer. *Cell* **88**, 747–756 (1997).
- Moon, R. T., Brown, J. D., Yang-Snyder, J. A. & Miller, J. R. Structurally related receptors and antagonists compete for secreted Wnt ligands. *Cell* **88**, 725–728 (1997).
- Wehrli, M. *et al.* *arrow* encodes an LDL-receptor-related protein essential for Wingless signalling. *Nature* **407**, 527–530 (2000).
- Tamai, K. *et al.* LDL-receptor-related proteins in Wnt signal transduction. *Nature* **407**, 530–535 (2000).
- Pinson, K. I., Brennan, J., Monkley, S., Avery, B. J. & Skarnes, W. C. An LDL-receptor-related protein mediates Wnt signalling in mice. *Nature* **407**, 535–538 (2000).
- Masiakowski, P. & Yancopoulos, G. D. The Wnt receptor CRD domain is also found in MusK and related orphan receptor tyrosine kinases. *Curr. Biol.* **8**, R407 (1998).
- Xu, Y. K. & Nusse, R. The Frizzled CRD domain is conserved in diverse proteins including several receptor tyrosine kinases. *Curr. Biol.* **8**, R405–406 (1998).
- Leahy, D. J., Dann, C. E., Longo, P., Perman, B. & Ramyar, K. A mammalian expression vector for expression and purification of secreted proteins for structural studies. *Protein Expr. Purif.* **20**, 500–506 (2000).
- Hendrickson, W. A. Determination of macromolecular structures from anomalous diffraction of synchrotron radiation. *Science* **254**, 51–58 (1991).
- Dauter, Z., Dauter, M. & Rajashankar, K. R. Novel approach to phasing proteins: derivatization by short cryo-soaking with halides. *Acta Crystallogr. D* **56**, 232–237 (2000).
- Holm, L. & Sander, C. Dali: a network tool for protein structure comparison. *Trends Biochem. Sci.* **20**, 478–480 (1995).
- Murzin, A. G., Brenner, S. E., Hubbard, T. & Chothia, C. SCOP: a structural classification of proteins database for the investigation of sequences and structures. *J. Mol. Biol.* **247**, 536–540 (1995).
- Orengo, C. A. *et al.* CATH—a hierarchic classification of protein domain structures. *Structure* **5**, 1093–1108 (1997).
- Lawrence, M. C. & Colman, P. M. Shape complementarity at protein/protein interfaces. *J. Mol. Biol.* **234**, 946–950 (1993).
- Hsieh, J. C., Rattner, A., Smallwood, P. M. & Nathans, J. Biochemical characterization of Wnt–frizzled interactions using a soluble, biologically active vertebrate Wnt protein. *Proc. Natl Acad. Sci. USA* **96**, 3546–3551 (1999).
- Wells, J. A. Systematic mutational analyses of protein–protein interfaces. *Methods Enzymol.* **202**, 390–411 (1991).
- Otwiniowski, Z. & Minor, W. Processing of X-ray diffraction data collected in oscillation mode. *Methods Enzymol.* **276**, 307–326 (1997).
- Terwilliger, T. C. & Berendzen, J. Automated MAD and MIR structure solution. *Acta Crystallogr. D* **55**, 849–861 (1999).

25. Zhang, K. & Main, P. Histogram matching as a new density modification technique for phase refinement and extension of protein molecules. *Acta Crystallogr. A* **46**, 41–46 (1990).
26. Jones, T., Zou, J.-Y., Cowan, S. & Kjeldgaard, M. Improved methods for building protein models in electron density maps and the location of errors in these models. *Acta Crystallogr. A* **47**, 110–119 (1991).
27. Brunger, A. T. *et al.* Crystallography & NMR system: a new software suite for macromolecular structure determination. *Acta Crystallogr. D* **54**, 905–921 (1998).
28. Carson, M. Ribbons 2.0. *J. Appl. Crystallogr.* **24**, 961–985 (1991).
29. Nielsen, H., Engelbrecht, J., Brunak, S. & von Heijne, G. Identification of prokaryotic and eukaryotic signal peptides and prediction of their cleavage sites. *Protein Eng.* **10**, 1–6 (1997).
30. Nicholls, A., Sharp, K. A. & Honig, B. Protein folding and association: insights from the interfacial and thermodynamic properties of hydrocarbons. *Proteins* **11**, 281–296 (1991).

Supplementary information is available on Nature's World-Wide Web site (<http://www.nature.com>) or as paper copy from the London editorial office of Nature.

**Acknowledgements**

We thank J. Beneken, K. Ramyar, C. Ogata and the staff at X4A for help with data collection; Z. Dauter for advice and technical assistance with phase determination using solvent halides; and D. Andrew, P. Beachy, J. Berg, J. Taipale and W. Yang for comments on the manuscript. Structures reported are accession numbers 1IJX for sFRP-3 and 1IJY for mFz8. Supported by the Howard Hughes Medical Institute.

Correspondence and requests for materials should be addressed to D.J.L. (e-mail: [leahy@groucho.med.jhmi.edu](mailto:leahy@groucho.med.jhmi.edu)).

**Mitochondrial endonuclease G is important for apoptosis in *C. elegans***

Jay Parrish\*, Lily Li†, Kristina Klotz\*, Duncan Ledwich\*, Xiaodong Wang† & Ding Xue\*

\* Department of Molecular, Cellular, and Developmental Biology, University of Colorado, Boulder, Colorado 80309, USA

† Howard Hughes Medical Institute and Department of Biochemistry, University of Texas Southwestern Medical Center, Dallas, Texas 75390, USA

Programmed cell death (apoptosis) is a tightly regulated process of cell disassembly in which dying cells and their nuclei shrink and fragment and the chromosomal DNA is degraded into internucleosomal repeats<sup>1–3</sup>. Here we report the characterization of the *cps-6* gene, which appears to function downstream of, or in parallel to, the cell-death protease CED-3 of *Caenorhabditis elegans* in the DNA degradation process during apoptosis. *cps-6* encodes a homologue of human mitochondrial endonuclease G<sup>4,5</sup>, and its protein product similarly localizes to mitochondria in *C. elegans*. Reduction of *cps-6* activity caused by a genetic mutation or RNA-mediated interference (RNAi) affects normal DNA degradation, as revealed by increased staining in a TUNEL assay, and results in delayed appearance of cell corpses during development in *C. elegans*. This observation provides *in vivo* evidence that the DNA degradation process is important for proper progression of apoptosis. CPS-6 is the first mitochondrial protein identified to be involved in programmed cell death in *C. elegans*, underscoring the conserved and important role of mitochondria in the execution of apoptosis.

Genetic analyses in *C. elegans* have led to the identification of several genes that are important for activation of programmed cell death (*egl-1*, *ced-3*, *ced-4* and *ced-9*), engulfment of cell corpses and degradation of DNA from the dead cells (*nuc-1*)<sup>6</sup>. However, little is known about what functions downstream of, or in parallel to, the activated CED-3 death protease to execute highly organized and efficient cell disassembly. To identify these missing links in the cell-death pathway, we carried out a sensitized genetic screen to isolate suppressors of a constitutively activated CED-3 mutant (acCED-3; D.L. and D.X., unpublished observations). In this screen, acCED-3 and green fluorescence protein (GFP) were co-expressed under the

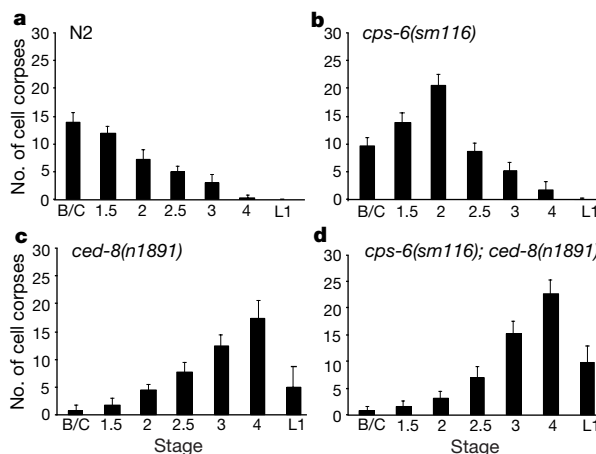


**Figure 1** *cps-6(sm116)* causes delayed appearance of cell corpses during development. Cell corpses were scored in the following animals: **a**, N2; **b**, *cps-6(sm116)*; **c**, *ced-8(n1891)*; **d**, *cps-6(sm116); ced-8(n1891)*. Stages of embryos or larvae examined were: bean and comma (B/C), 1.5-fold (1.5), 2-fold (2), 2.5-fold (2.5), 3-fold (3), 4-fold (4) and early L1 larvae (L1). The definition of the stages of embryos is as described<sup>8</sup>. The y axis represents the average number of cell corpses scored in the head regions of embryos or larvae. Error bars are the standard error of the mean (s.e.m.). At least 15 embryos were counted for each developmental stage.

control of the promoters of the *mec-7* and *mec-3* genes ( $P_{mec-7}$  and  $P_{mec-3}$ ), respectively, in six non-essential mechanosensory neurons<sup>7</sup>, and GFP was used as a sensitive cell-existence marker to select for mutants in which neuronal deaths induced by acCED-3 are delayed or partially suppressed. As shown in Table 1, expression of acCED-3 in animals homozygous for an integrated array (*smIs1*) containing both  $P_{mec-7}$ -acCED-3 and  $P_{mec-3}$ -GFP constructs induced most (>84%) of the six mechanosensory neurons to undergo apoptosis. We further sensitized this screen by introducing a mutation, *n1891*, into the *ced-8* gene of the *smIs1* animals, which results in a general delay of cell death<sup>8</sup> and also partial suppression of acCED-3-induced neuronal deaths (Table 1). We then looked for mutations that could enhance the death-suppressing effect of *ced-8(n1891)*.

From one such screen of 3,000 mutagenized haploid genomes (see Methods), we identified a single recessive mutation, *sm116*, that significantly enhanced the suppression of acCED-3-mediated neuronal deaths by *ced-8(n1891)* (Table 1). *sm116* alone was also a weak suppressor. We found that *sm116* identifies a new locus on chromosome I, which was named *cps-6* (CED-3 protease suppressor).

To investigate whether *sm116* affects normal programmed cell death in nematodes, we performed a time-course analysis of embryonic cell corpses<sup>8</sup>. In wild-type animals, the peak of cell corpses appears in the bean or comma embryonic stage, while in the *ced-8(n1891)* mutant, the peak of cell corpses shifts to the four-fold embryonic stage, showing an overall delay in cell-corpse

**Table 1** *cps-6(sm116)* enhances suppression of acCED-3-mediated neuronal deaths by *ced-8(n1891)*

Strain*	No. of animals	AVM†	ALMR/L†	PVM†	PLMR/L†
<i>smIs1</i>	50	16%	14%	10%	0%
<i>smIs1; ced-8(n1891)</i>	40	35%	8%	25%	0%
<i>cps-6(sm116); smIs1</i>	52	23%	24%	17%	1%
<i>cps-6(sm116); smIs1; ced-8(n1891)</i>	60	63%	35%	37%	3%

\* *smIs1* was generated by integrating through exposure to  $\gamma$ -rays an extrachromosomal array containing  $P_{mec-7}$ -acCED-3 (10  $\mu$ g ml<sup>-1</sup>),  $P_{mec-3}$ -GFP (10  $\mu$ g ml<sup>-1</sup>) and pL15EK (40  $\mu$ g ml<sup>-1</sup>), a plasmid that rescues *lin-15* mutant<sup>9</sup>, into *lin-15(n765ts)* animals. It was then backcrossed six times with N2 animals and mapped to LGV.

† The percentage of mechanosensory neurons with GFP in L4 larvae is shown, which was scored using a fluorescent Nomarski microscope. AVM, ALMR/L, PVM and PLMR/L are six mechanosensory neurons.